Bulletin of the
Seismological Society of America

Vol. 77 December 1987 No. 6

RESULTS FROM A 1500 M DEEP, THREE-LEVEL DOWNHOLE SEISMOMETER ARRAY: SITE RESPONSE, LOW Q VALUES, AND f_{max}

BY EGILL HAUKSSON, TA-LIANG TENG, AND THOMAS L. HENYEY

ABSTRACT

A three-level downhole array is being operated in a 1500-m-deep borehole within the seismically active Newport-Inglewood fault zone, Los Angeles basin. The array consists of three three-component 4.5 Hz seismometers deployed at the surface, and at 420 and 1500 m depth. An M = 2.8 earthquake that occurred 0.9 km away from the array at a depth of 5.3 km on 31 July 1986 generated rays traveling almost vertically up the downhole array. The P- and S-wave pulse shapes show increasing pulse rise time with decreasing depth, and the initial pulse slope is less steep at the surface than at 1500 m. The average value of t_s/t_p between 1500 and 420 m depth is 1.7 and between 420 and 0 m is 3.4. A near-surface site response results in amplification on the P wave by a factor of four and S waves by a factor of nine. These data indicate a near-surface Q_α of 44 ± 13 for rays traveling almost vertically. In the case of S waves, most of the high frequency content of the waveform beyond ~10 Hz observed at 1500 m depth is lost through attenuation before the waveform reaches 420 m depth. The average Q_β is 25 ± 10 between 1500 and 420 m depth and 108 ± 36 between 420 and 0 m depth. The spectra of the S waves observed at 420 and 0 m of the downward reflected S phases may overestimate Q_β, because they are limited to a narrow band between 5 and 10 Hz and affected by the near-surface amplification. A Q_c of 160 ± 30 at 6 Hz was determined from the decay rate of the coda waves at all three depths. The corner frequency as determined from displacement spectra may be higher (f_c ~ 10 Hz) at 1500 m depth than at (f_c ~ 7 Hz) 420 and 0 m depth. Similarly, f_{max} significantly decreases as the waveforms travel toward the earth's surface, indicating that f_{max} is affected by near-surface attenuation. Beyond f_c, the average slopes of the spectra falloff of P-wave spectra is ~f^{-2} at 1500 m depth and ~ f^{-3} at the surface.

INTRODUCTION

A three-level downhole seismometer array with seismometer sondes at the surface, and at 420 and 1500 m depth has been installed in a deep abandoned oilwell in the Baldwin Hills, Southern California. The Baldwin Hills are cross-cut by the Newport-Inglewood fault zone, a major earthquake fault in the Los Angeles basin (Yerkes *et al.*, 1965; Hauksson, 1987; Figure 1). The downhole seismometer array is designed to record seismic waves from local earthquakes to study near-surface attenuation and site response such as amplification of seismic waves.

Numerous investigators have suggested that surface recordings of local earthquakes and hence the source parameter determinations are contaminated by attenuation of high frequencies and/or dominated by a narrow band of frequencies amplified through reverberation close to the earth's surface (e.g., Frankel, 1982; Hanks, 1982; Archuleta *et al.*, 1982; Cranswick *et al.*, 1985). Downhole seismometer arrays should be able to provide data to quantify such effects. In addition to

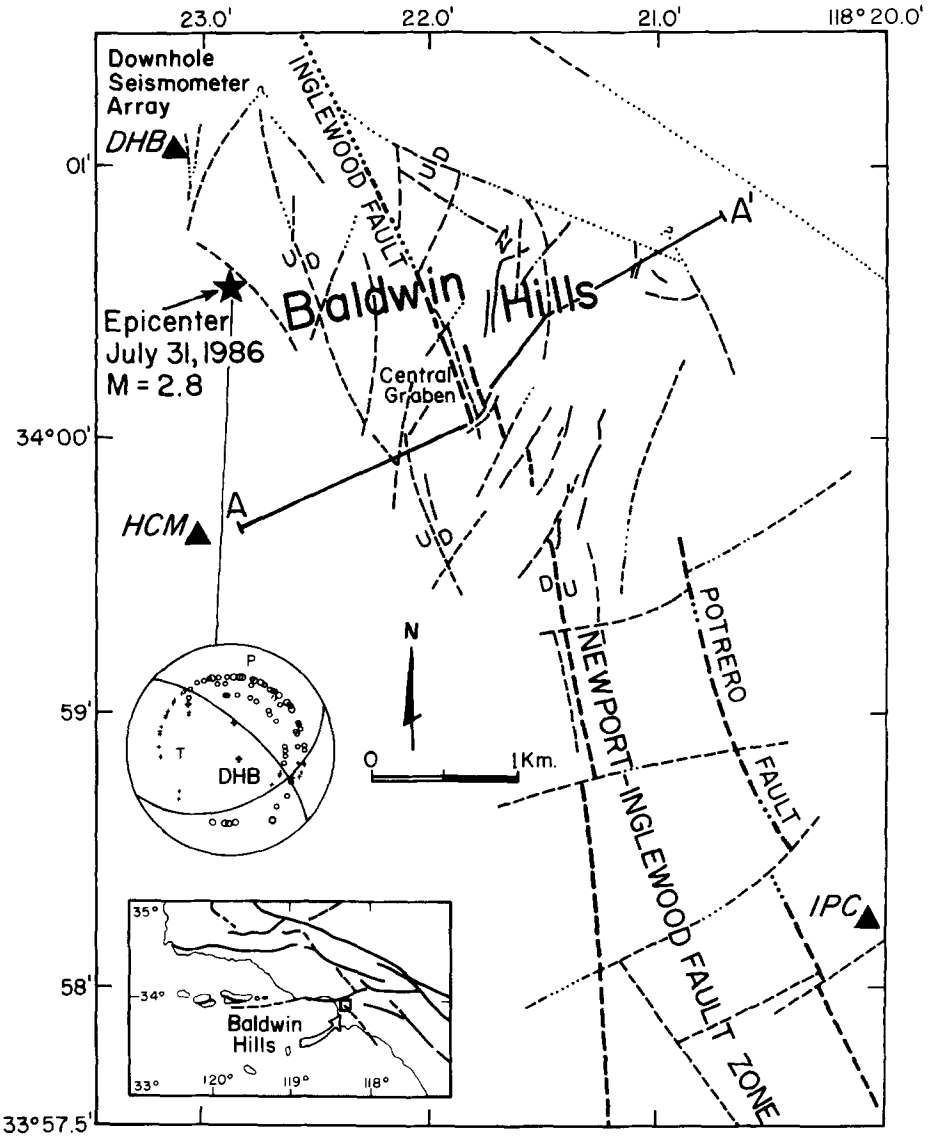

FIG. 1. Map showing the location of the three-level downhole seismometer array with respect to the Newport-Inglewood fault zone. (*Lower left*) Map of southern California (*inset*) showing the Baldwin Hills located at the north end of the Newport-Inglewood fault zone. The focal mechanism is a lower-hemisphere solution including first-motion polarities with + indicating up and open circle indicating down motion. Data are from both USC and CIT/USGS seismic networks. (*Upper left*) The three-level downhole seismometer array (DHB) and the epicenter of the 31 July 1986 event shown as a star. HCM and IPC are nearby surface seismic stations operated by USC. Fault traces are from Hart (1980).

attenuation of P and S waves, the attenuation of coda waves needs to be studied using data from downhole arrays to identify the source region of the coda generation (Phillips and Aki, 1986).

The near-surface P- and S-wave velocities in the Los Angeles basin are low and thus separate in time the downgoing phases from upcoming phases, as recorded by the borehole array at shallow depths. Furthermore, the near-surface attenuation is high and should have a pronounced effect on the recorded seismograms. The near-surface velocity and sedimentary structures (Figure 2) have also been mapped in

detail while exploring for oil (Wright *et al.*, unpublished data, 1973). The frequent occurrence of small earthquakes along the Newport-Inglewood fault zone provides sources at a variety of incident angles as well as distance to the array (Hauksson, 1987). Such sources can be used to measure near-surface attenuation and site response to provide, for instance, an alternate technique to mapping of S-wave velocity at shallow depths using artifical seismic sources (e.g., Tinsley and Fumal, 1985).

Most previous studies have examined downhole seismograms from shallow boreholes of depth less than 150 m. The results are often inconclusive because the waveforms can be severely contaminated by downward-reflected phases resulting in destructive interference and making the spectra of the downhole seismograms anomalously deficient in certain frequencies (Andrews and Borcherdt, 1986; Archuleta, 1986). Studies from deeper boreholes of depth 150 to 500 m, however, do not suffer from such interference and have shown that low Q values are found at shallow depths (e.g., Malin and Walker, 1985).

In this paper, seismograms from one earthquake (M = 2.8) that occurred 900 m south of the array at a depth of 5.3 km on 31 July 1986 are analyzed. The seismograms of the event are unusual in that they mainly consist of vertical rays. The near vertically traveling rays of this event virtually eliminate the effect of incident angle. Converted phases at layer interfaces appear to be absent, while the surface reflections have large amplitudes and can be easily identified in the seismograms as distinct arrivals that have symmetric travel times.

The results presented here show low near-surface (above 1500 m depth) Q values that cause strong attenuation of high frequencies for both P and S waves. These

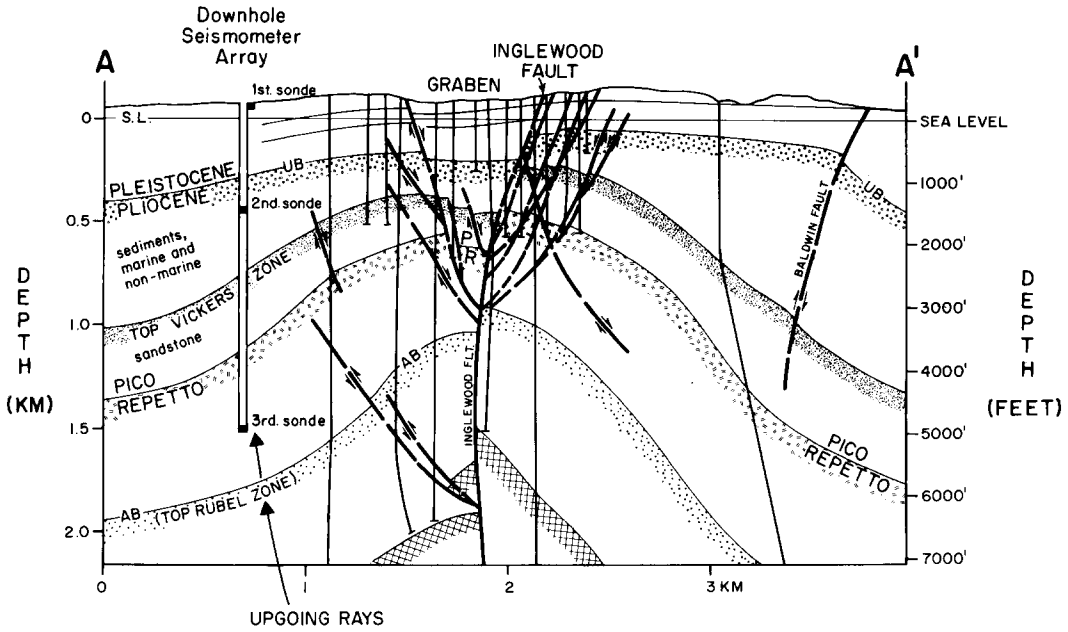

FIG. 2. A cross-section (A-A', Figure 1) of the Baldwin Hills (Wright *et al.*, unpublished data 1973). The three-level downhole seismometer array is shown to the *left*. Thin almost vertical lines indicate approximate positions of boreholes and corresponding logs that were used to construct this section. For details of the stratigraphy see Yerkes *et al.* (1965) and Wright *et al.* (unpublished data, 1973). The "Top Vickers Zone" is the oil-bearing sandstone formation. The thick lines indicate the Inglewood fault and other near-surface subsidiary faults.

low Q values and spectra of waveforms recorded at 1500 m depth suggest that f_{max} may be primarily a near-surface site effect rather than a source effect. The high-frequency background earth noise (including cultural, wind, and microseism noise) as recorded by the downhole array decays in amplitude exponentially with depth. Hence, by deploying instruments deeper than 1000 m in the Los Angeles basin, it is possible to avoid the high levels of background earth noise and to record waveforms before they are depleted in high frequencies by strong near-surface attenuation.

Instrumentation and Data Analysis

The Baldwin Hills borehole was made available to the University of Southern California (USC) Geophysics Laboratory in 1972 by Chevron Oil Company and has been used as a single- or two-component seismograph station in the USC Los Angeles basin seismic network. In late 1985, efforts were begun to reinstrument the borehole. The details of the current instrumentation are shown in Figure 3. Each sonde consists of a stainless steel downhole package containing a three-component Marks Products L-1B-HT 4.5 Hz seismometer. The L-1B-HT seismometers can withstand the bottom hole temperature of 84°C. The surface sonde is installed on a concrete pier 3 m from the borehole. The sonde at 420 m depth is clamped to the borehole wall using a spring-loaded lever arm. The sonde on the bottom of the borehole at 1500 m depth rests in place on its own weight.

The borehole penetrates the Quaternary and Tertiary sediments of the Los Angeles basin as shown in Figure 2. The bottom sonde at 1500 m depth is located well within the "Top Vickers" zone of late Tertiary oil bearing sandstone. The marine and nonmarine sediments around the second sonde at 420 m depth are of Pliocene age. The surface sediments around the borehole consist of irregular mixtures of poorly consolidated flood-plain deposits such as gravels, sand, and clays (Yerkes *et al.*, 1965; Wright *et al.*, unpublished data 1973).

The seismic data are transmitted over phone lines using an Optimum Telemetry System (OTS) developed at USC. The OTS transmits the vertical component signal in real-time to the central recording station at USC. If an earthquake is detected by the the OTS at the site, the OTS stores all three components on scale by gain-ranging. It then transmits the three components sequentially with the gain-ranged signals delayed by 30 sec (Teng and Hsu, 1986). The final recording is accomplished at 100 sps by a PDP $\frac{11}{34}$ that is used by the USC Los Angeles basin seismic network.

One of the advantages of placing an array of instruments in deep boreholes is to gain further understanding of how rapidly background earth noise levels decrease with depth (Takahashi *et al.*, 1984). The borehole needs to be deep enough to provide a reduction in the background noise to compensate for the lost signal amplification caused by the near-surface amplification. Low background noise levels permit detecting smaller earthquakes and high fidelity recording of moderate-sized events on scale. The length of the time window selected for spectral analysis of the earth noise was 2.56 sec (Figure 4). The peak in noise at 420 m depth and 20 Hz may be instrument-related, since it is not always reproduced by taking time windows of noise data recorded by different amplifiers. The noise level decreases most rapidly in the near-surface layers and has decayed by 28 dB at 420 m depth relative to the surface. The rate of decay is similar over the whole frequency band of 2 to 30 Hz. An additional 10 dB decrease in noise level is obtained by increasing the instrument depth from 420 to 1500 m. Observations of earth noise in 3000 m deep boreholes in Tokyo, Japan, show approximately the same rate of decay with depth (Takahashi

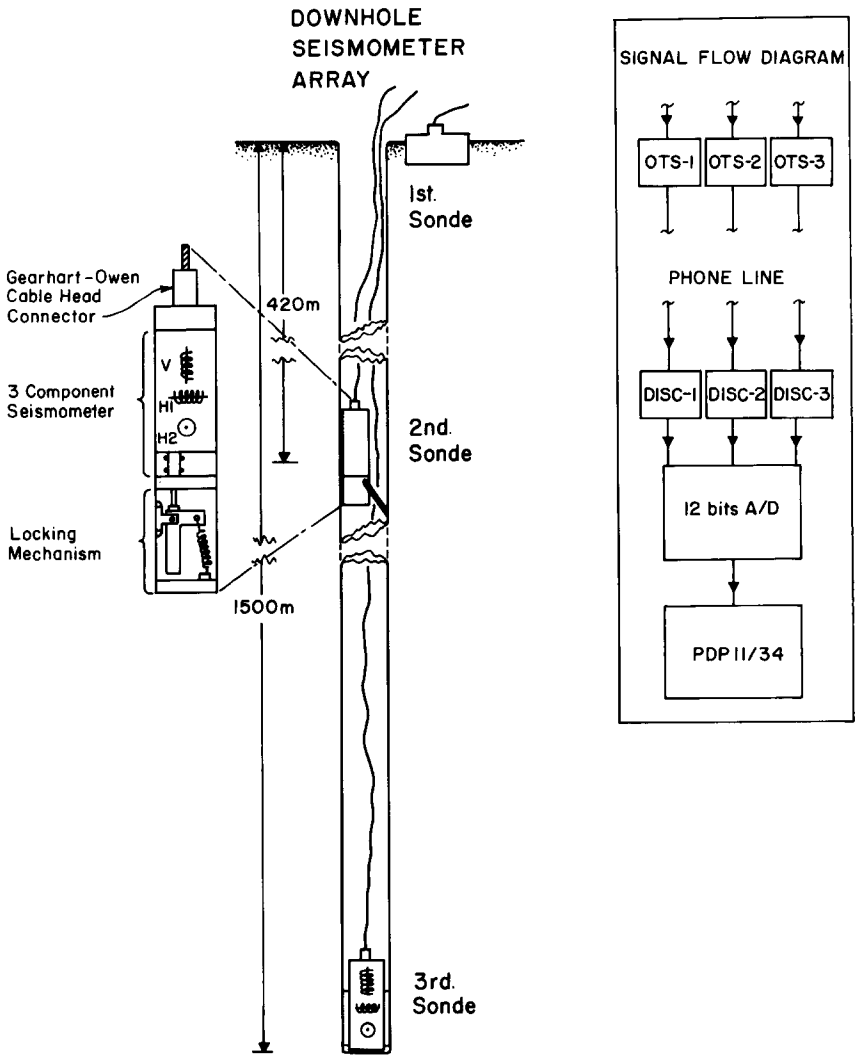

FIG. 3. A schematic illustration of the three-level downhole seismometer array. Each sonde contains a 4.5 Hz three-component seismometer L-1B-HT. The surface sonde is mounted on a concrete pier. The sonde at 420 m depth is clamped to the borehole casing using a spring-loaded lever arm. The sonde at 1500 m is placed on the bottom of the borehole and rests in place on its own weight. (*Right*) Signal flow diagram for signals from the seismometers, which pass through OTS, phone lines, discriminators (DISC), and an analog-to-digital converter (A/D). The signals are event-detected and recorded by a PDP $\frac{11}{34}$ computer.

et al., 1984). Hence, most of the noise reduction is gained between 0 and 420 m depth, while deploying instruments as deep as 1500 m makes it possible to record the seismograms before they are attenuated by the near-surface layers.

Initially, the seismograms are corrected for gain and the fixed OTS time delay. The horizontal components are rotated to obtain radial and transverse components. Because the azimuths of the downhole horizontal seismometers are unknown, the rotation is based on: (1) the amplitude of the first cycle of the P wave; (2) consistent polarities for P and S waves; and (3) similarities with the oriented surface seismograms. The resulting uncertainty range in the orientation of the horizontal components is on the order of 20° to 30°. This large uncertainty does not affect the conclusions of this study.

The hypocenter of the (M = 2.8) earthquake of 31 July 1986 (Figure 1) was calculated using the program, HYPOINVERSE (Klein, 1985). The fault-plane solution (Figure 1) includes first-motion data from both the USC Los Angeles basin network and the CIT/USGS southern California seismic network, and was determined using the program, FPFIT (Reasenberg and Oppenheimer, 1985). The hypocentral parameters and P- and S-arrival times for the borehole array are listed in Table 1.

The spectral analyses of waveforms were done using standard Fast Fourier transforms. Each spectrum was corrected for the frequency response of the 4.5 Hz seismometer using a similar approach as discussed by Stewart and O'Neill (1980). The calculated response curves were also compared with measured response curves

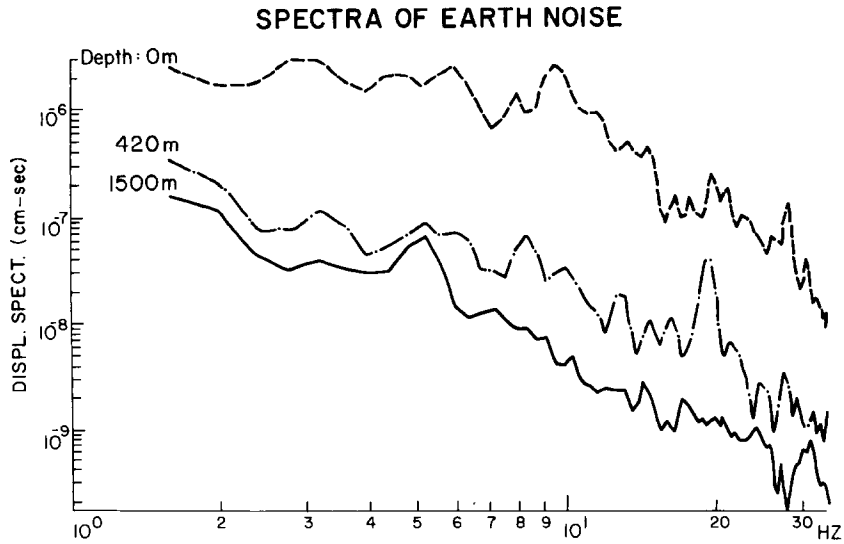

FIG. 4. Displacement (DISPL.) spectra of high-frequency earth noise at 0, 420, and 1500 m depth as recorded by the three-level downhole seismometer array in the Baldwin Hills, Los Angeles basin. The time window is 2.56 sec of noise data from each vertical component. The earth noise decreases most rapidly in the 0 to 420 m depth range.

TABLE 1

HYPOCENTRAL PARAMETERS AND P-WAVE ARRIVAL TIMES RECORDED WITH THE THREE-LEVEL DOWNHOLE ARRAY FOR THE 31 JULY 1986 (M = 2.8) EARTHQUAKE

Date	Time (UTC)		Location			Focal Mechanism*		
			Latitude (°N)	Longitude (°W)	Depth (km)	Ddir	Dip	Rake
31 July 1986	1916	46.09	34 0.6	118 22.9	5.3	155	45	30

Sonde Depth (m)	P (sec)	S (sec)	M_0† (dyne-cm)	r† (m)	$\Delta\sigma$† (bars)	r‡ (m)	σ‡ (bars)
0	47.37	48.96	$1.0 \cdot 10^{20}$	160	10	320	0.5
420	47.12	48.10	$0.6 \cdot 10^{20}$	160	14	290	2.5
1500	46.68	47.34	$0.4 \cdot 10^{20}$	110	32	260	2.8

* Ddir = dip direction of nodal plane in degrees; dip = dip of nodal plane in degrees; rake = rake of the focal mechanism in degrees.

† From displacement spectra where M_0 is seismic moment, r is source radius, and $\Delta\sigma$ is static stress drop.

‡ From P-wave pulse (in Figure 13) where r is source radius and σ is dynamic stress drop.

obtained from the manufacturer of the seismometers. The time window of 0.64 sec has a 10 per cent cosine taper. Only the spectra included in the spectral ratios are smoothed by using a smoothing routine published by Robinson (1983).

RESULTS

On 31 July 1986, the downhole seismometer array recorded a local earthquake (M = 2.8) at an epicentral distance of 900 m and a depth of 5.3 km. The ray path between the source and receiver deviates less than 10° from vertical as is shown in the fault-plane solution (Figure 1). This particular geometry of having a source directly beneath the borehole array is unusual and results in simple seismograms.

The three-component seismograms in Figure 5 demonstrate the strong attenua-

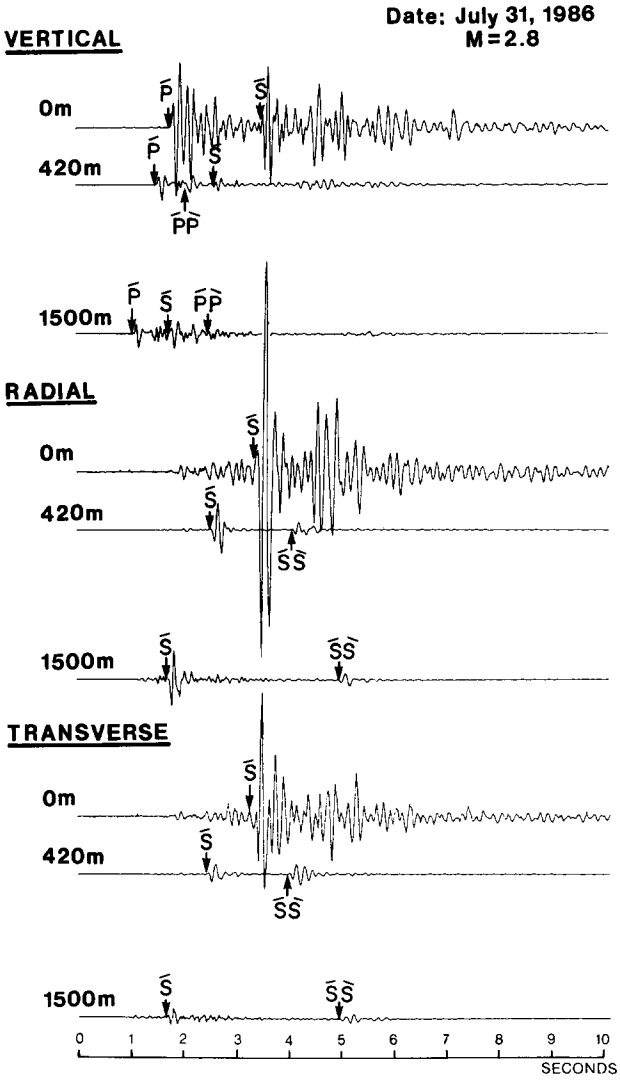

FIG. 5. The rotated seismograms of the (M = 2.8) 31 July 1986 earthquake that were recorded by the downhole seismometer array plotted in a time versus depth plot at correct relative gains. The upcoming phases are labeled $\acute{P}$ or $\acute{S}$, and downgoing phases are labeled $\grave{P}\grave{P}$ or $\grave{S}\grave{S}$. The notation of acute and grave accents (Aki and Richards, 1980) indicates the sequence of upcoming and downgoing waves. The surface seismograms (0 m) have larger amplitudes because of near-surface amplification. These seismograms are also shown normalized peak to peak in Figures 7 to 9.

tion of P and S waves. The upcoming and downgoing S waves recorded by the same seismometer can be visually compared to evaluate relative frequency content. Hence, the main result of this paper, that both P and S waves at shallow depths have been depleted in high frequencies, is obvious from visually inspecting the seismograms. To put this result into a familiar framework and to quantify this variation in frequency content as a function of recording depth, several accepted data analysis techniques are applied.

Site response. The three-component seismograms in Figure 5 are shown in a time versus depth plot. The horizontal components have been rotated into approximate radial and transverse components as previously discussed. Since they are plotted at the same gain, they demonstrate near-surface amplification of P waves by a factor of four and S waves by a factor of nine. This site effect results from low elastic moduli of the unconsolidated near-surface sediments in the Los Angeles basin.

The P wave ($\acute{P}$) traveling from depth toward the surface can be seen arriving sequentially first at 1500 m, then at 420 m, and finally at 0 m depth. A corresponding downgoing P wave ($\acute{P}\grave{P}$) that is reflected off the free surface can be seen on the vertical seismograms, in particular at the 420 m depth. The S waves that are observed most clearly on the radial and transverse components form a similar symmetric pattern of upcoming direct waves ($\acute{S}$) and downgoing surface-reflected waves ($\acute{S}\grave{S}$). The large depth of the array and the slow near-surface velocities result in the large time separation between direct and reflected phases, which in turn eliminates constructive or destructive interference of upcoming and downgoing waves.

A curve of sonic travel-time versus depth for the Baldwin Hills is shown on the left in Figure 6 (Teng *et al.*, 1973). The P-wave arrival times at 420 and 1500 m relative to the arrival time at 0 m depth are also plotted in Figure 6. The observed P arrivals show low apparent velocities consistent with the travel-time curve that was obtained from sonic logging using vertically traveling rays. A velocity model corresponding to the travel-time curve indicates a smoothly increasing velocity with depth (Figure 6). The relative arrival times of the P and S waves at different levels

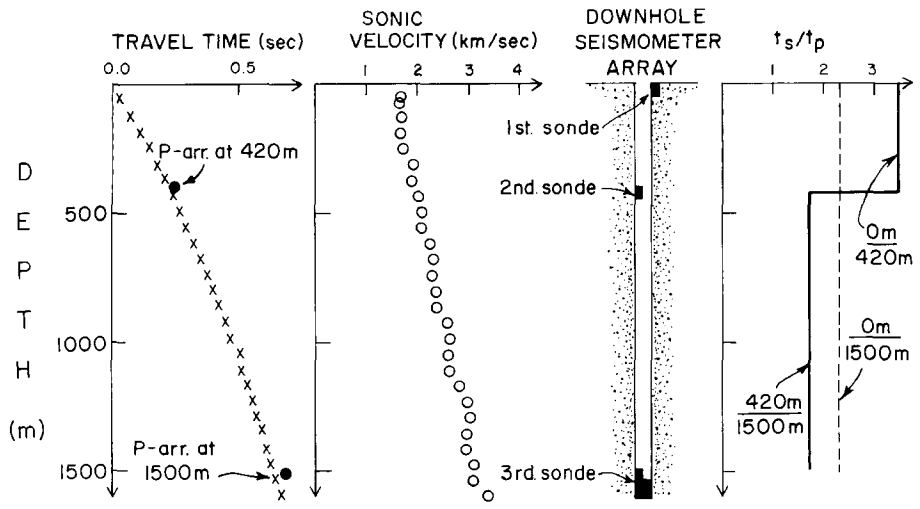

FIG. 6. (*Left*) A general travel-time curve for the Baldwin Hills (Teng *et al.*, 1973) and the relative P arrivals (arr.) at 420 and 1500 m depth. (*Center*) A gradient velocity model derived from the travel-time curve. (*Right*) t_s/t_p ratio determined from the recorded P- and S-wave arrivals of the 31 July 1986 earthquake.

of the borehole array are a direct measure of the V_p/V_s ratio for the near-surface layers around the borehole. The average value of t_s/t_p between 0 and 1500 m depth is 2.3, while the value between 420 and 1500 m depth is 1.7 and 0 and 420 m depth is 3.4 (Figure 6).

Near-surface attenuation. The downhole seismometer array provides a measure of the attenuation of P, S, and coda waves near the earth's surface. The near-surface attenuation can be determined from the formula

$$A(Z, f) \cdot Z = A(Z_0, f) \cdot Z_0 \cdot \exp(-\alpha(Z - Z_0)) \tag{1}$$

where

$$\alpha = (\pi \cdot f)/(Q \cdot V)$$

and

$$Q = (\pi \cdot (t - t_0))/(\log_e 10 \cdot m)$$

and $A(Z, f)$ is the observed spectral amplitude, Z is the distance from source to receiver, Z_0 is a reference distance, f is the frequency, V is velocity, Q is the quality factor, and $t = Z/V$ or $t_0 = Z_0/V$ is the travel time of P or S waves (Båth, 1974). Because the travel times, t, are available, these are used to determine Q instead of making assumptions about the velocity structure. The slope, m, of the log of spectral ratio versus frequency is inversely proportional to Q as can be seen from the aforementioned formula. To determine Q for P or S waves traveling up the borehole array, spectral ratios between averaged spectra of waveforms recorded at different depths in the borehole are calculated.

The formula (1) assumes that the geometrical spreading factor is proportional to $1/Z$, where Z is distance from source to receiver. To evaluate the applicability of this assumption, a geometrical spreading factor was calculated using a layered velocity structure derived for the Los Angeles basin by Teng *et al.* (1973) and a ray theory approach by Newman (1973). The spreading factors from ray theory are approximately equal to $1/Z$ for the depth range of the borehole array, but for the 2-5.3 km depth range they are approximately equal to $1/(2.5 \cdot Z)$. Hence, for determining Q in the 0 to 1500 m depth range of the borehole array, the geometrical spreading factor of $1/Z$ is sufficient.

The vertical component seismograms are shown normalized peak-to-peak in Figure 7 (top). The 0.64 sec time window around the P arrival that was chosen for spectral analysis is indicated by a horizontal bar. The corresponding P-wave displacement spectra are also shown in Figure 7 (center). For the purposes of clean plotting, the spectrum of the P wave recorded at 1500 m depth is offset by one decade relative to the 420 and 0 m spectra. The 420 and 1500 m spectra have similar spectral levels at low frequencies (less than 10 Hz). The 420 and 0 m spectra, however, are offset by a factor of four, which constitutes the near-surface amplification. The rate of spectral fall-off beyond the corner frequency of 7 to 10 Hz ranges from $f^{-2.2\pm0.5}$ at 1500 m depth to $f^{-3.0\pm0.4}$ at the surface, indicating high near-surface attenuation for P waves. The attenuation of the P waves is determined from the slope of the spectral ratios shown in Figure 7 (bottom). The Q_α values that are similar for the two depth intervals (1500 to 420 m) and (420 to 0 m) are 43 ± 13

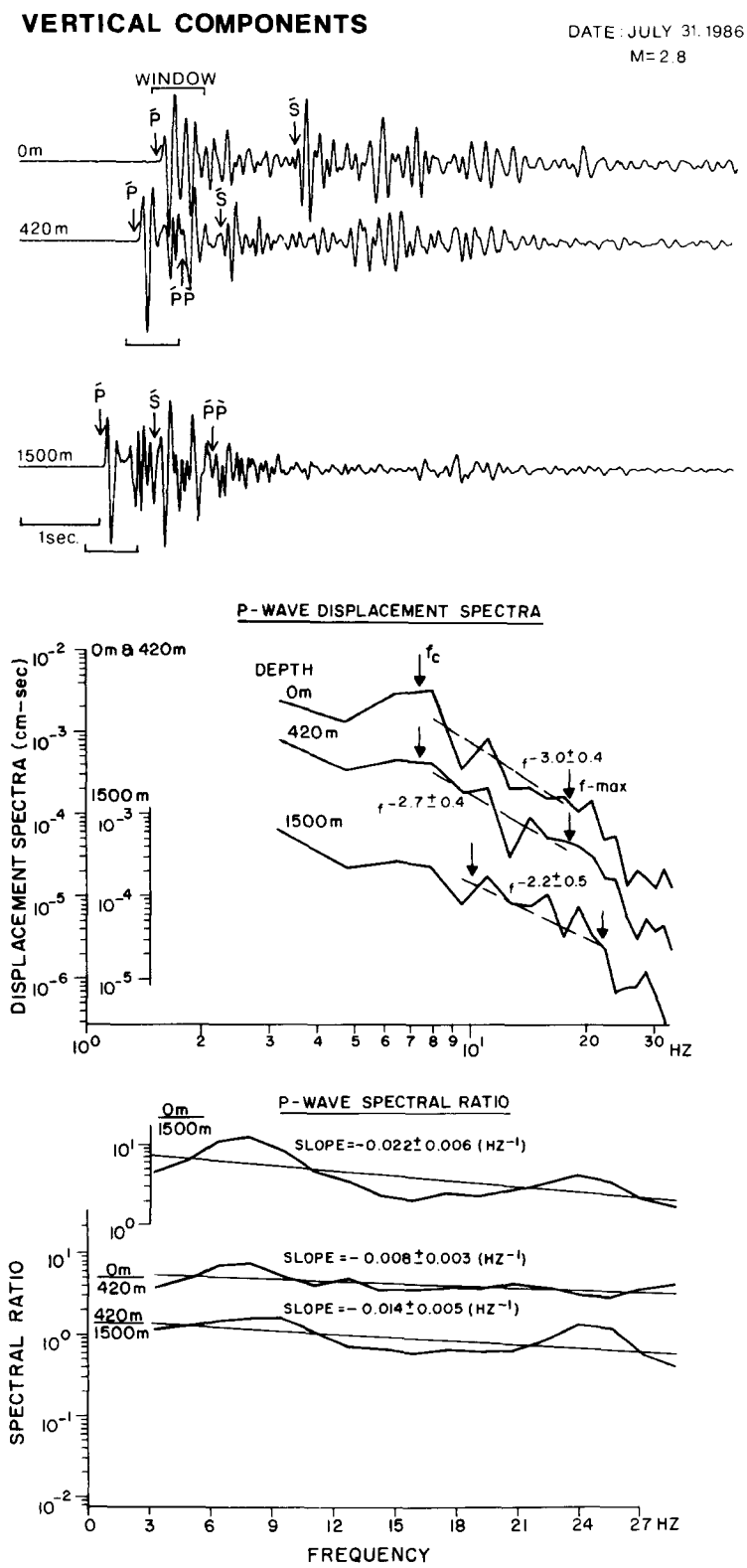

FIG. 7. (*Top*) The vertical component seismograms normalized peak to peak to show the details of the waveform. The time window selected for spectral analysis is indicated by a 0.64-sec-long horizontal bar. (*Center*) The corresponding *P*-wave displacement spectra where the vertical scale of the 1500 m depth spectrum is offset by one decade relative to the 0 and 420 m spectra. The fall-off rate of the high-frequency end is calculated for the range of 8 to 24 Hz. The corner frequency, f_c, and f_{max} are indicated by arrows. (*Bottom*) Smoothed *P*-wave spectral ratios for 420/1500, 0/420, and 0/1500 m spectra. The slope is calculated for the range of 3 to 30 Hz. The 0/1500 m ratio is offset to avoid overlapping plots.

and 45 ± 13, respectively. The $Q\alpha$ for the whole length of the array (0 to 1500 m) gives an average value of 44 ± 13. Q_α is low in the depth range of 0 to 1500 m, but remains consistent with the observed velocity structure.

Plots of normalized seismograms, displacement spectra, and spectral ratios for radial and transverse components of S waves, similar to those for P waves, are shown in Figures 8 and 9. The rate of spectral fall-off beyond the corner frequency (7 to 10 Hz) up to 20 Hz for SV waves is $f^{-3.0\pm0.9}$ at 1500 m depth and $f^{-4.0\pm0.4}$ at the surface. Similarly, for SH waves, the rate of spectral fall-off ranges from $f^{-3.1\pm0.4}$ at 1500 m depth of $f^{-4.5\pm0.4}$ at the surface, indicating high attenuation for S waves. At frequencies higher than 20 Hz, the S waves are contaminated by the P-wave coda which changes the slope of the high-frequency end of the displacement spectra and could make the spectral ratios above 20 Hz meaningless.

Figures 8 and 9 show a significant difference between the waveforms of the S waves recorded at 1500 m depth versus those at 420 and 0 m depth. The waveforms recorded at 420 and 0 m depth are similar in frequency content but are both depleted in high frequencies relative to the waveforms recorded at 1500 m depth. Most of the observed high-frequency content of the waveform beyond the corner frequency (10 Hz) at 1500 m depth is lost through attenuation before the waveform reaches 420 m depth. Q_β for SV waves is approximately 30 ± 10 for the depth interval 1500 to 420 m, while Q_β for SH waves is approximately 20 ± 10. Because the orientations of the downhole horizontal seismometers are uncertain, an average Q_β for SH and SV waves is determined. The average Q_β in the depth interval of 1500 to 420 m is 25 ± 10.

The Q_β in the depth range of 420 to 0 m cannot be easily determined because of the high-surface amplification. The slopes of the spectral ratios in Figures 8 and 9 for spectra recorded at 420 and 0 m depth are small and suggest that Q_β between 420 m depth and the surface is much greater than Q_β in the depth range of 1500 to 420 m. One possible explanation for the small slopes is the effect of near-surface amplification on the surface seismograms. If the near-surface amplification is frequency-dependent, it would distort the spectral slopes.

To avoid the interference of the near-surface amplification with the determination of Q_β, the spectra of the $\acute{S}$ and $\acute{S}\grave{S}$ waves recorded at 420 m depth have been determined (Figure 10). The spectra of the background signal or coda are also included in Figure 10 to indicate that above approximately 10 to 15 Hz the signal strength of the $\acute{S}$ and $\acute{S}\grave{S}$ waves is similar to background signal strength. Hence, the high frequencies have been removed from the $\acute{S}$ and $\acute{S}\grave{S}$ waves and attenuated or transformed into scattered coda. The spectral ratios of radial and transverse components of the $\acute{S}$ and $\acute{S}\grave{S}$ waves are shown in Figure 10 (bottom). The Q_β for the transverse component is 94 ± 24 and for the radial component 123 ± 47 or an average Q_β is 108 ± 36, when using the spectral slopes in the frequency range of 3 to 20 Hz. The transverse component has a higher signal to noise ratio than the radial component and therefore the one standard deviation error bars are smaller than for the radial component.

Based on spectral slopes of the $\acute{S}$ and $\acute{S}\grave{S}$ waves, the Q_β in the depth range 420 to 0 m is approximately four to five times larger than Q_β in the depth range of 1500 to 420 m. It is possible that the downgoing $\acute{S}\grave{S}$ wave that is generated by the free surface reflection is still contaminated by near-surface amplification or ray focusing, which results in overestimating the Q_β. This observation of high Q_β in the depth range of 420 to 0 m and low Q_β in the depth range of 1500 to 420 m may also be real, and may reflect the presence of fluids such as oil and gas (at depths greater than 420 m) in the sediments of the Inglewood oilfield.

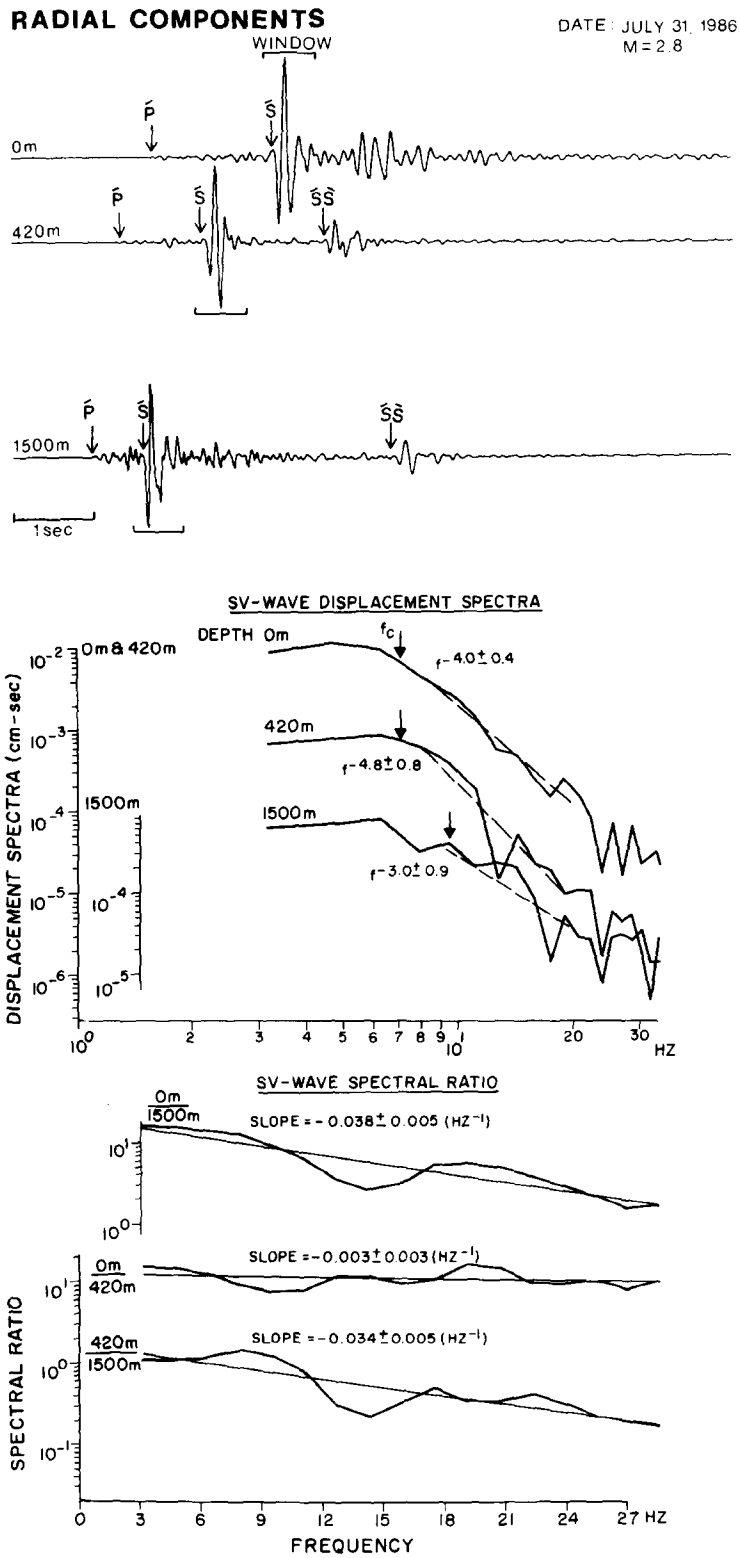

FIG. 8. (*Top*) The radial component seismograms normalized peak to peak to show the details of the waveform. The time window selected for spectral analysis is indicated by a 0.64-sec-long horizontal bar. (*Center*) The corresponding *SV*-wave displacement spectra where the vertical scale of the 1500 m depth spectrum is offset by one decade relative to the 0 and 420 m spectra. The rate of fall-off of the high-frequency end is calculated for the range of 8 to 20 Hz. The corner frequency, f_c, is indicated by arrows. (*Bottom*) Smoothed *SV*-wave spectral ratios for 420/1500, 0/420, and 0/1500 m spectra. The slope is calculated for the range of 3 to 30 Hz. The 0/1500 m ratio is offset to avoid overlapping of the spectral ratios.

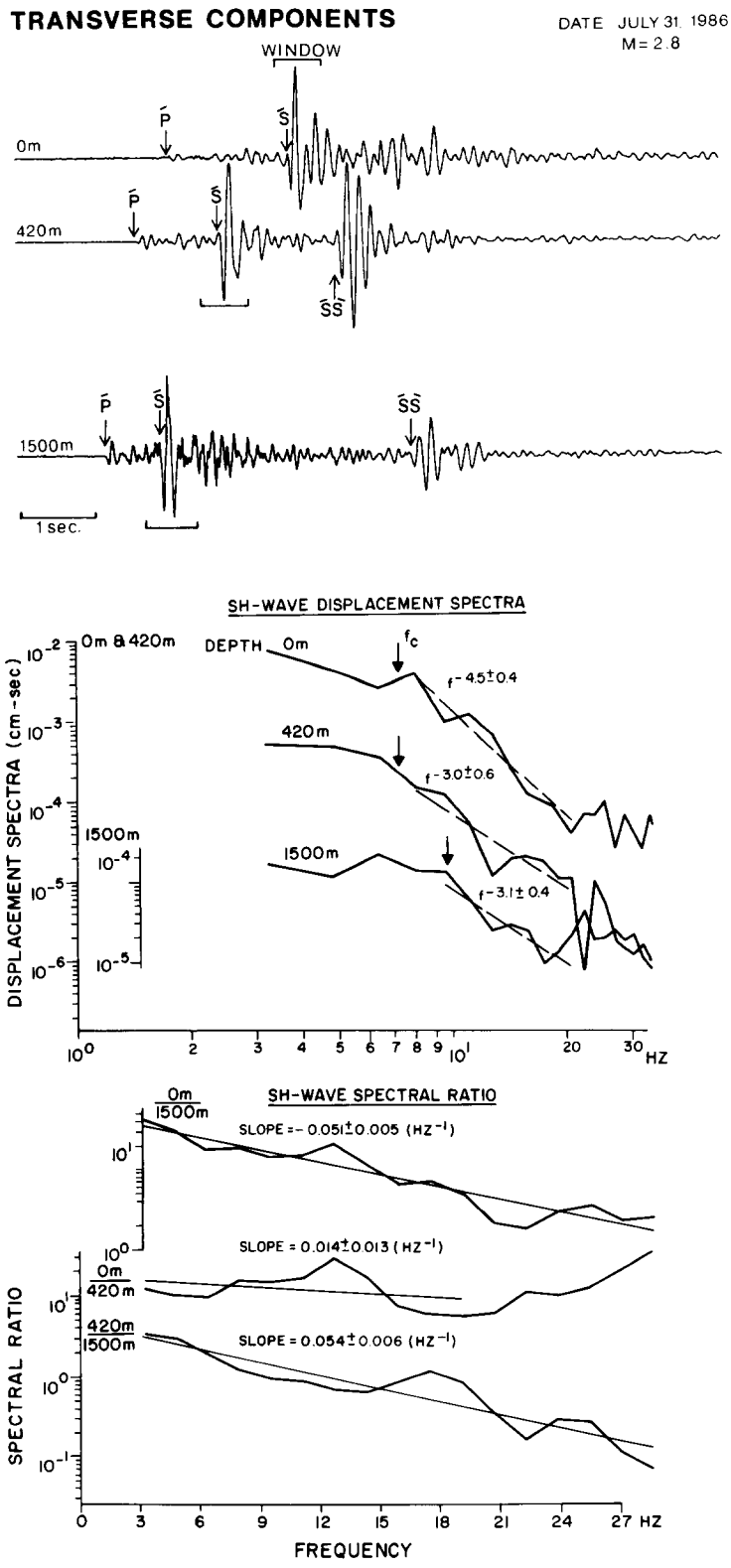

FIG. 9. (*Top*) The transverse component seismograms normalized peak to peak to show details of the waveform. (*Center*) The corresponding *SH*-wave displacement spectra. (*Bottom*) Smoothed *SH*-wave spectral ratios for 420/1500, 0/420, and 0/1500 m spectra. (See also caption to Figure 8.)

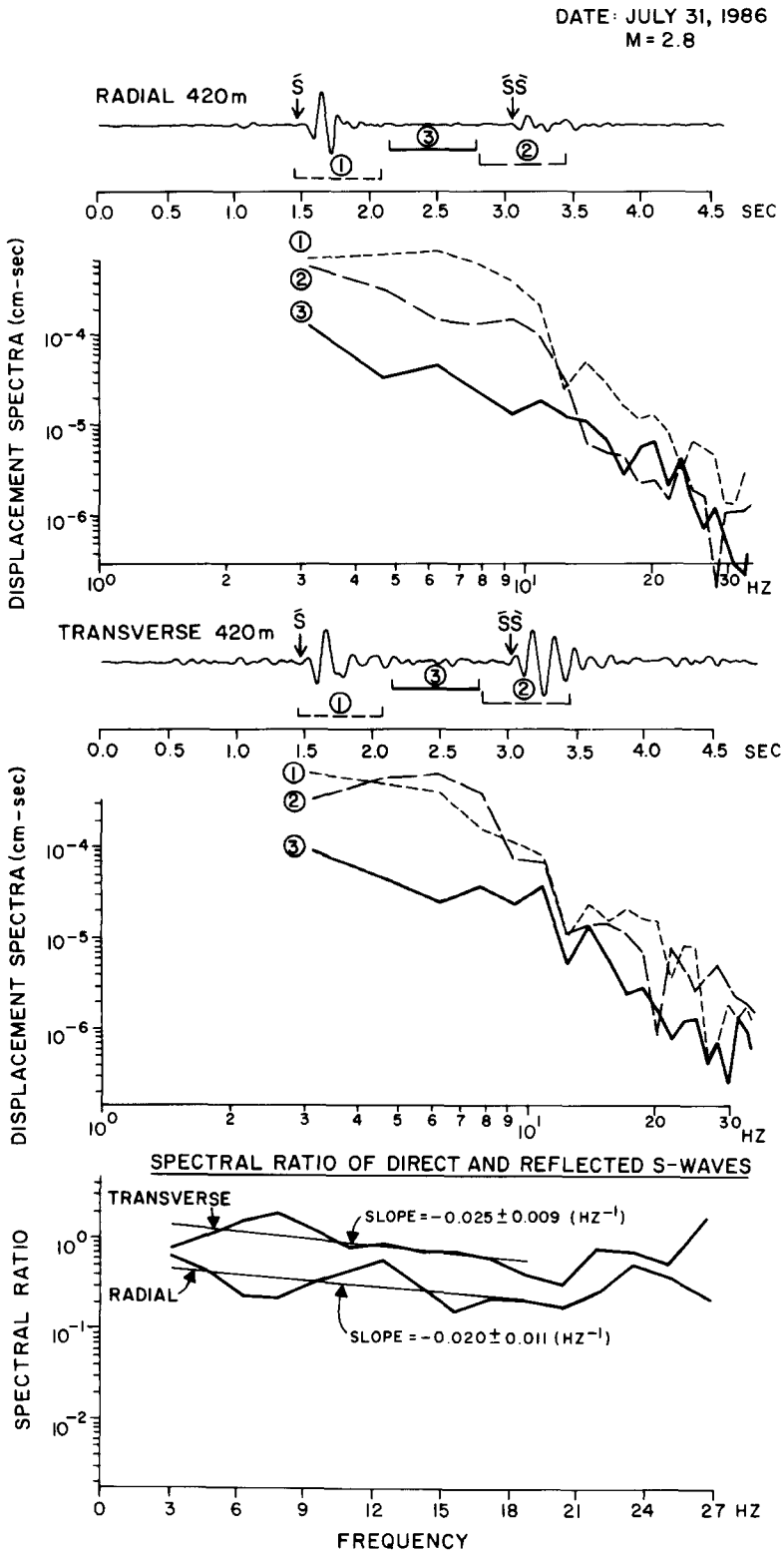

FIG. 10. (*Top*) The radial component seismogram recorded at 420 m depth and the displacement spectra of the $\hat{S}$ and $\hat{S}\hat{S}$ waves. The spectra and windows of $\hat{S}$ and $\hat{S}\hat{S}$ waves are labeled (1) and (2), respectively. Also shown is the spectrum of the background coda labeled (3). (*Center*) The transverse component seismogram recorded at 420 m depth and displacement spectra of $\hat{S}$ and $\hat{S}\hat{S}$ waves and background coda labeled (1), (2), and (3), respectively. (*Bottom*) Corresponding spectral ratios of spectra of $\hat{S}$ and $\hat{S}\hat{S}$ waves for both radial and transverse components. The slope is calculated for the frequency range of 3 to 20 Hz.

Coda Q, or Q_c, was determined for the three levels of the borehole. The vertical component seismograms shown in Figure 11 are normalized on the first P arrival in amplitude and then compressed to show the rate of decay with time of the coda following the S waves. The coda in seismograms recorded at 0, 420, and 1500 m depth have approximately the same overall amplitude and rate of decay with time. The Q_c was calculated using the formula

$$(A(f/t) \cdot t)^2 \sim \exp(-2 \cdot \pi \cdot f \cdot t \cdot Q_c^{-1})$$

where $A(f/t)$ is spectral amplitude, t is travel time, f is frequency, and Q_c is coda Q (Aki and Chouet, 1975). Discrete spectral windows were taken beyond twice the S travel time and $A(f \mid t) \cdot t$ was plotted versus t in a log-linear plot. The slope in this plot is proportional to Q_c and gave similar Q_c values for 0, 420, and 1500 m depth. Averaged over the seismograms recorded at three different depths, the Q_c is 160 ± 30 at 6 Hz.

Summary plots of Q_α, Q_β, and Q_c as a function of depth are shown in Figure 12. The similar Q_c values at all three depths may imply that the coda is mostly scattered body waves rather than surface waves. The higher Q_c than Q_α or Q_β and the longer travel path for coda waves suggests that scattering and reverberations in the basin sediments at distances up to 20 to 30 km away from the borehole contribute to Q_c. Further studies of Q_c, Q_α, and Q_β using sources with different angles of incidence are needed to understand the relative importance of anelastic attenuation versus scattering as well as the mechanisms of coda generation.

Corner frequency and f_{max}. The displacement spectra shown in Figures 7 to 9 can also be used to determine the corner frequency and $f_{\max}$ for this earthquake. The corner frequency is defined as the point of intersection between the tangents to the almost flat, low-frequency spectral level and the high-frequency fall-off. The uncertainty in determining the corner frequency is rather high since the data are bandlimited in frequency to 3 to 30 Hz. Nonetheless, there is some suggestion in

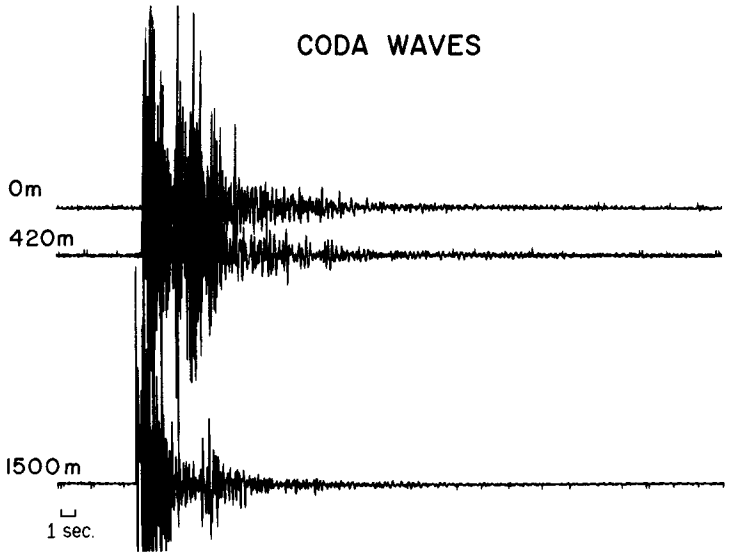

FIG. 11. Vertical component seismograms that are normalized peak to peak and compressed in time to show the rate of coda decay.

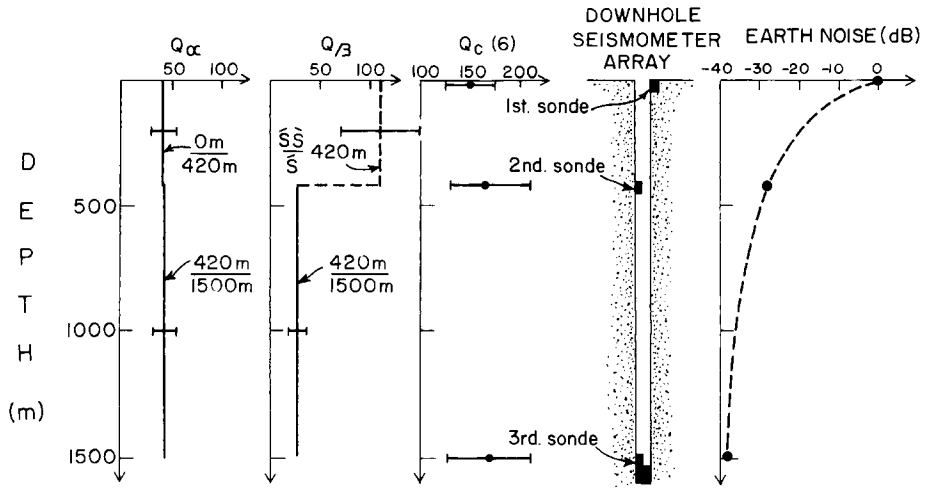

FIG. 12. A summary of observed Q_α, Q_β, and Q_c as a function of depth. Note Q_β in the depth range of 420 to 0 m is calculated using the S and SS spectral ratio, which may overestimate Q_β because the depletion of high frequencies from the S waves and near-surface amplification does not permit accurate determination of Q_β. Also shown is the average high-frequency earth noise as a function of depth.

Figures 7 to 9 that the corner frequency is higher ($f_c \cong 10$ Hz) at 1500 m depth than at 420 and 0 m where $f_c \cong 7$ Hz.

Based on Brune's (1970) formulation for a circular fault and assuming $V_s \cong 3.0$ km/sec, $\rho = 2.7$ gm/cm^3, and correction for radiation pattern of 0.7, the source parameters (seismic moment, source radius, and stress drop) are derived (Table 1). Using the seismogram recorded at the surface, where the correction for near-surface amplification is 9.0 for S waves, and the average SV and SH corner frequency is 7 Hz, yields a seismic moment of $M_0 = 1.0 \cdot 10^{20}$ dyne-cm, a source radius of $r = 160$ m, and a static stress drop of $\sigma = 10$ bars. Similarly, using the seismograms recorded at 1500 m depth, where there is no surface correction but the corner frequency is 10 Hz, yields $M_0 = 0.6 \cdot 10^{20}$ dyne-cm, $r = 110$ m, and $\sigma = 32$ bars. Therefore, the source radius estimate as inferred from the 1500 m seismograms is smaller, and the static stress drop estimate is higher than those inferred from the surface seismograms.

Similarly, f_{max} (defined here as the frequency above which the spectra fall-off rate is greater than the fall-off rate immediately following f_c) is higher at 1500 m depth than at 420 or 0 m depth. In the case of P waves, the value of f_{max} is approximately 22 Hz at 1500 m and at 420 m but approximately 18 Hz at the surface. The S waves do not show a reduction in f_{max} because the high-frequency end ($f > 20$ Hz) of the S-wave spectra appear to flatten out in Figures 8 and 9, caused by possible contamination from scattered P-wave coda. The reduction in f_{max} and P-wave coda contamination is reflected in the spectral ratios for S waves in Figures 8 and 9.

P-wave pulse shapes. The shape of the initial P-wave pulse can be used to derive source parameters such as source radius and dynamic stress drop (e.g., Boatwright, 1980; Frankel, 1982). Source parameters obtained from seismograms recorded by the downhole seismometer array can be extrapolated back to zero travel time and thus corrected for path attenuation.

In Figure 13, the P-wave pulses for the 31 July 1986 earthquake are plotted at correct gain levels and superimposed such that the initial P-wave onsets coincide in time. The surface (0 m) trace is most prominent because the near-surface

amplification increases the signal amplitude by a factor of four. This plot demonstrates that the initial pulse duration (from the P-wave onset to the first zero-crossing) increases as the P-wave travels the length of the array.

Both the pulse duration (τ_D) and the pulse rise time (τ_R) can be used as a measure of attenuation (Figure 14). Ohtake (1987), who measured P-wave pulse durations to search for temporal changes in Q_α, used the formula

$$\tau_D = \tau_i + C \cdot t \cdot Q\alpha^{-1}$$

where τ_i is the initial pulse width, C is a constant (assumed to be equal to 1.0), and t is travel time. In Figure 14, the pulse duration is plotted versus travel time. Because only three data points are available, this plot is only intended as a schematic illustration of how the initial source duration can be determined. In this case, a minimum source duration of 50 msec is obtained, which corresponds approximately to a source radius of 200 m using a formula derived by Boatwright (1980) and assuming a rupture velocity of $(0.7 \cdot V_s)$. The P-wave duration of 80 msec measured at the surface (0 m) corresponds to a source radius of 320 m (Table 1).

A similar approach that was discussed by Kjartansson (1979) uses the pulse rise time (τ_R) to determine Q_α, using the formula

$$\tau_R = \tau_0 + C \cdot t \cdot Q_\alpha{-}1$$

where τ_0 is the pulse rise time at the source, t is the travel time, and $C = 0.485$ for Q_α greater than 20. The Q_α value determined with this formula is 28 (Figure 14). The three Q_α values that were determined using the spectral ratio, pulse duration, and pulse rise time thus range from 28 to 44.

Figure 14 (bottom) shows the average slope of the P-wave pulse plotted versus

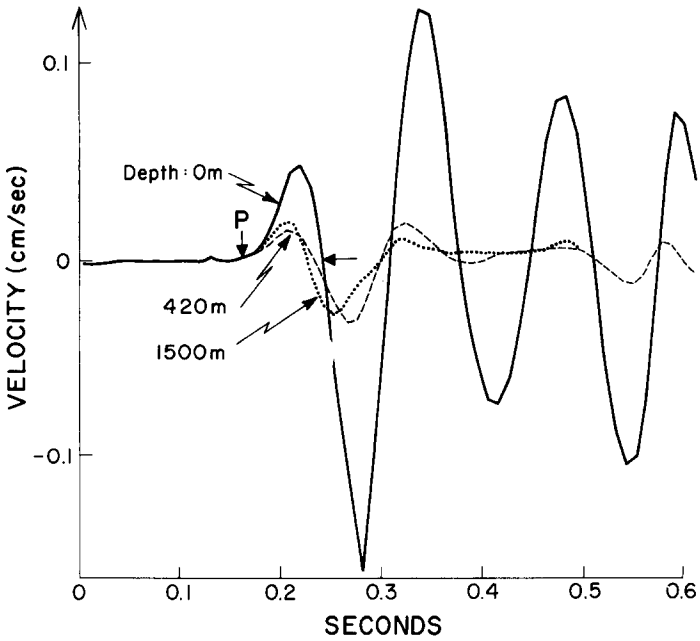

FIG. 13. The P-wave pulses that were recorded at 1500, 420, and 0 m depth are plotted at correct gain to illustrate how the first pulse broadens as the P wave travels up toward the surface.

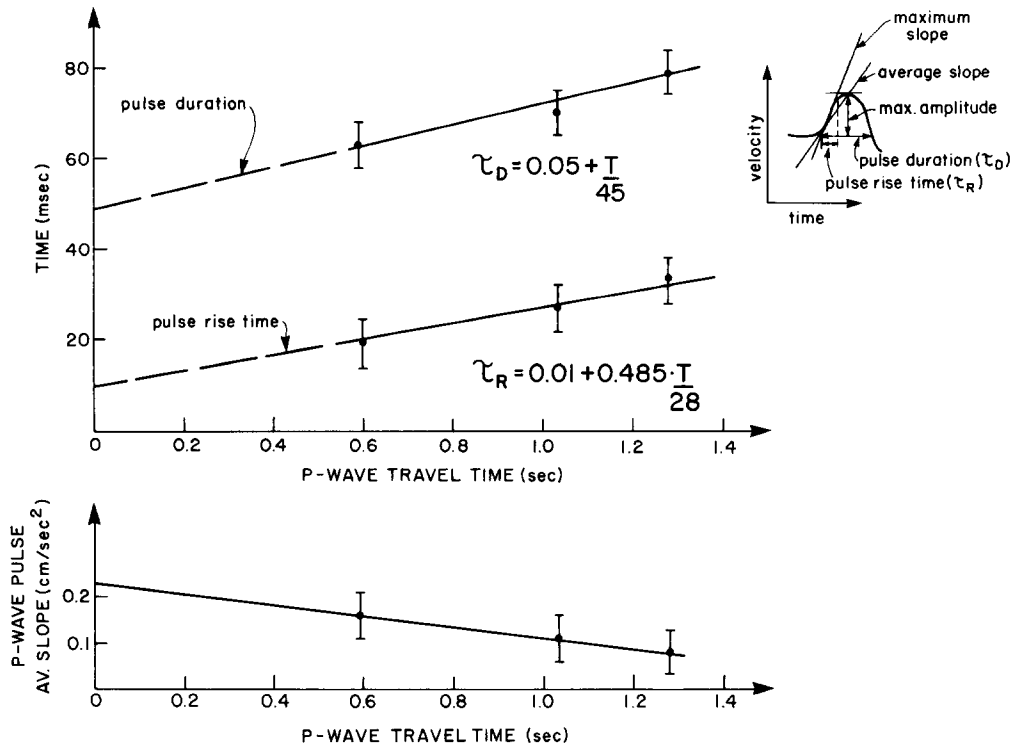

FIG. 14. (*Top left*) *P*-wave pulse duration and rise time versus travel time. (*Top right*) Schematic illustration of how maximum slope, average slope, pulse duration, and pulse rise time are defined. The formulas (*center right*) are explained in the text. (*Bottom*) The average slope of the *P*-wave pulses versus travel time.

travel time. Before determining the slope of the *P*-wave pulse at the surface (0 m), the amplitude was corrected for the near-surface amplification. The slope of 0.22 cm/sec^2 corresponds to dynamic stress drop of greater than 3 bars (Boatwright, 1980). The slope of the *P*-wave pulse at the surface (0 m), however, yields a dynamic stress drop of 0.5 bars when accounting for geometrical spreading and near-surface effects (Table 1). The source radius and dynamic stress drop determined from the *P*-wave pulse are smaller than the radius and stress drop determined from the *S*-wave spectra. This may result from Q_α being greater than Q_β as well as from different assumptions inherent in both techniques.

The Q_α determined from the increase in *P*-wave pulse duration is 45 and from pulse rise time is 28 (Figure 14), which is similar to the Q_α determined from the spectral ratios in Figure 7. It should be noted that the high attenuation along the borehole array causes the duration to almost double following 1.5 sec of travel time. Hence, studies that use data from surface instruments alone and do not correct for attenuation may overestimate the source radius. Since the stress drop scales with the source radius, it may be underestimated when using only surface data.

DISCUSSION

Site response. The prediction of strong ground motion from potentially damaging earthquakes requires knowledge of possible site response or near-surface amplification that may result from low elastic moduli in the near-surface sediments. Bard and Gabriel (1986) calculated the seismic response of two-dimensional sedimentary basins with vertical velocity gradient. They found near-surface amplification of *SH*

waves up to a factor of ten. To determine the near-surface site amplification, Rogers *et al.* (1984) deployed instruments in the Los Angeles basin and recorded seismic waves from Nevada nuclear tests. They compared the nuclear test recordings with strong motion data from the 1971 San Fernando earthquake and found that both recordings produced similar spectral levels at a given site. Spectra for alluvial sites divided by a spectrum from a crystalline rock site showed near-surface amplification of factor of two to ten in the frequency range of 0 to 5 Hz. Similarly, Joyner *et al.* (1976) reported that near-surface amplification of a factor of four or five was recorded by a four-level downhole array in the mud sediments in southwest San Francisco Bay.

The results of this study show a near-surface amplification of a factor of four for P waves and a factor of nine for S waves. The large t_s/t_p ratio demonstrates that the S-wave velocity is at least a factor of two lower than would be expected from a t_s/t_p ratio of 1.73. Therefore, the larger near-surface amplification for S waves than for P waves is consistent with the *in situ* low S-wave velocities (200 to 530 m/sec) measured in shallow boreholes in the Los Angeles basin by Tinsley and Fumal (1985). Furthermore, the P pulses in Figure 13 show that attenuation of high frequencies (pulse-broadening) and amplification over a broad frequency band caused by impedance change with depth (amplified peak amplitude) are not incompatible. Further analysis of local earthquake data from the downhole array are needed to establish if a local earthquake transfer function can be used to separate attenuation and amplification effects, and can be used as a stable measure of site response.

Q values. The Q_α and Q_β determined from the spectral ratios in this study are assumed to be independent of frequency. Using P-wave pulse shapes, Kjartansson (1979) derived a linear model of wave propagation and attenuation with Q independent of frequency. He demonstrated that models based on Q as a function of frequency do not provide a better fit to available data than models based on Q independent of frequency. Several studies (e.g., Aki and Chouet, 1975; Aki, 1980; Singh *et al.*, 1982), however, have shown that Q_β in some cases is a function of frequency (1 to 25 Hz). To resolve the frequency dependence of Q, more advanced data analysis techniques are required than are used in this study. For instance, Singh *et al.* (1982) compared recorded *SH* spectra with spectra from synthetic seismograms to determine the Q_β structure along the Imperial fault. They found Q_β of 57 to 100 in the upper 4 km of crust but could not resolve the frequency dependence of Q_β. At depths greater than 4 km, the Q_β was frequency-dependent along the Imperial fault and ranged from 70 to 140 (at 5 to 10 Hz) and from 400 to 500 (at 20 to 25 Hz).

The borehole data presented in this study are collected in the Los Angeles basin. The basin sediments are known to have low *in situ* P- and S-wave velocities and high attenuation (Tinsley and Fumel, 1985). The Q_α and Q_β obtained here, however, are not unusually low for near-surface sediments. Numerous previous studies of Q using borehole or surface instruments have provided similarly small values. Recently, Malin and Waller (1985) recorded seismograms at five different levels in a 0.5 km deep borehole at Oroville, California. They found unusually low Q_β of 3 and 9 within and above the Cleveland Hills fault that intersects the borehole at approximately 300 m depth. Joyner *et al.* (1976) used data from a four-level downhole array to determine Q_β of 16 in the uppermost 186 m of sediments on the southwest shore of San Francisco Bay. Low near-surface Q_β (60 to 120) was also obtained by Barker and Stevens (1983) who measured Q_β in the uppermost 100 m of sediments

in the Imperial Valley, California. As previously discussed, Singh *et al.* (1982) also found low Q_β (57 to 100) along the Imperial fault for depths less than 4 km. Bakun and Bufe (1975), who used seismograms of local earthquakes near the San Andreas fault in central California, reported low Q_β (75 to 100) for the frequency range (1 to 12 Hz). The agreement between the results of this study and previous studies using either downhole or surface instruments thus illustrates that local earthquakes can be used successfully as seismic sources for determining near-surface Q.

f_{max}. The parameter $f_{\max}$ is used to describe the lack of high frequencies in source spectra of local earthquakes at frequencies somewhat greater than the corner frequency. $f_{\max}$ has been interpreted to be the result of either source effects or near-surface path effects (e.g., Archuleta *et al.*, 1982; Hanks, 1982; Papageorgiou and Aki, 1983; Anderson and Hough, 1984; Anderson, 1986). Archuleta *et al.* (1982) argued that if $f_{\max}$ was a path effect, it was unusually repeatable and observed at nearly all locations throughout the world. They also pointed out that if it was a source effect, the laws of self-similarity (that describe the scaling of earthquake sources with magnitude) would be violated (Aki, 1967). To search for a possible path effect related to $f_{\max}$, Archuleta (1986) presented data from a 100 m deep borehole at McGee Creek near Mammoth Lakes in eastern California. His results, however, proved to be inconclusive because the borehole was not deep enough to record significantly different seismograms at the top and bottom of the borehole. Papageorgiou and Aki (1983) explicitly assumed that $f_{\max}$ was primarily a source effect related to anelasticity of the fault to derive a model to predict local ground motions. Hanks (1982) evaluated the possible origin of $f_{\max}$ and concluded that data from a borehole array such as are presented here were needed. High-quality borehole data could possibly resolve whether $f_{\max}$ is a source or path effect by documenting if the high frequencies that appear to be absent at the surface are detected at depth.

The most significant result of this study is the observation that the S waves recorded at 0 and 420 m depth have been depleted in high frequencies (greater than ~10 Hz) relative to S waves recorded at 1500 m depth. Both the decrease in corner frequency or $f_{\max}$ and the spectral ratios indicate that the high frequencies were removed by the high path attenuation between 1500 and 420 m. This result suggests that $f_{\max}$ is primarily a path effect.

To explain the fall-off of acceleration spectra at high frequency, Anderson and Hough (1984) demonstrated that the spectra exhibit exponential decay. They argued that the rate of decay, and thus $f_{\max}$, was not a source effect but rather a near-surface path effect related to high attenuation in the weathered layer. Their conclusions are consistent with the data from the downhole seismometer array.

CONCLUSIONS

A three-level downhole seismometer array operated in a 1500 m deep borehole in the Newport-Inglewood fault zone recorded on 31 July 1986 an $M = 2.8$ earthquake. Since the hypocenter was located at 5.3 km depth directly beneath the array, the seismograms of the event are unusual in that they mainly consist of vertical rays. The spectral ratio, P pulse rise time, and duration techniques provide similar values for Q_α (28 to 44). The spectral ratio technique was used to obtain $Q_\alpha = 44 \pm 13$ in the depth range of 0 to 1500 m and $Q_\beta = 25 \pm 10$ in the depth range of 420 to 1500 m. The Q_β in the depth range of 0 to 420 m cannot easily be determined because of the near-surface amplification. The spectral ratios of the $\acute{S}$ and $\acute{S}\acute{S}$ waves at 420 m depth, however, suggest that $Q_\beta = 108 \pm 36$ in the depth range of 0 to 420 m. The $Q_c = 160 \pm 30$ at 6 Hz was determined from the decay rate of the coda waves. The

low Q_β observed between 1500 and 420 m depth does not permit the high frequencies (greater than 10 Hz) only observed at 1500 m depth to reach the surface. This observation suggests that f_{max} may be primarily a path effect rather than a source effect. The near-surface attenuation affects the determination of source parameters of local earthquakes such that dynamic stress drops are underestimated, and source radius is overestimated in surface recordings.

ACKNOWLEDGMENTS

M. Roberston, D. Manov, and J. Scott helped design and install the downhole array and performed necessary technical maintenance. We thank K. Aki, an anonymous reviewer, and D. M. Boore for comments, and L. M. Jones, A Frankel, and P. E. Malin for reviews. This research was supported by U.S. Geological Survey Grant 14-08-0001-G1158, U.S. Geological Survey Contract 14-08-0001-A0264, and NSF Grants EAR-8407830 and EAR-8608997. The figures were drafted by J. Dodds and the manuscript typed by D. Moton and S. Turnbow.

REFERENCES

Aki, K. (1967). Scaling law of seismic spectrum, *J. Geophys. Res.* **72,** 1217–1231.

Aki, K. (1980). Attenuation of shear waves in the lithosphere for frequencies from 0.05 to 25 Hz, *Phys. Earth Planet. Interiors* **21,** 50–60.

Aki, K. and B. Chouet (1975). Origin of coda waves: source attenuation and scattering effects. *J. Geophys. Res.* **80,** 3322–3342.

Aki, K. and P. G. Richards (1980). *Quantitative Seismology: Theory and Methods*, W. H. Freeman, San Francisco, California, 948 pp.

Anderson, J. G. (1986). Implication of attenuation for studies of the earthquake source, in *Earthquake Source Mechanics*, Maurice Ewing Series, vol. 6, S. Das, J. Boatwright, and C. H. Scholz, Editors, American Geophysical Union, Washington, D.C., 311–318.

Anderson, J. G. and S. Hough (1984). A model for the shape of the Fourier amplitude spectrum of acceleration at high frequencies, *Bull. Seism. Soc. Am.* **74,** 1969–1994.

Andrews, M. C. and R. D. Borcherdt (1986). Response of near-surface geology from uphole-downhole arrays at Coalinga, California, *EOS, Trans. Am. Geophys. Union* **67,** 1091.

Archuleta, R. J. (1986). Downhole recordings of seismic radiation, in *Earthquake Source Mechanics*, Maurice Ewing Series, vol. 6, by S. Das, J. Boatwright, and C. H. Scholz, Editors, American Geophysical Union, Washington, D.C., 319–329.

Archuleta, R. J., E. Cranswick, C. Mueller, and P. Spudich (1982). Source parameters of the 1980 Mammoth Lakes, California, earthquake sequence, *J. Geophys. Res.* **87,** 4595–4607.

Bakun, W. H. and C. G. Bufe (1975). Shear-wave attenuation along the San Andreas fault zone in central California, *Bull. Seism. Soc. Am.* **65,** 439–459.

Bard, P.-Y. and J.-C. Gabriel (1986). The seismic response of two-dimensional sedimentary deposits with large vertical velocity gradients, *Bull. Seism. Soc. Am.* **76,** 343–366.

Barker, T. G. and J. L. Stevens (1983). Shallow shear wave velocity and Q structures at the El Centro strong motion accelerograph array, *Geophys. Res. Letters* **10,** 853–856.

Båth, M. (1974). *Spectral Analysis in Geophysics*, Elsevier Scientific Publishing Company, Amsterdam, The Netherlands, 563 pp.

Boatwright, J. (1980). A spectral theory for circular seismic sources: simple estimates of source dimension, dynamic stress drop, and radiated seismic energy, *Bull. Seism. Soc. Am.* **70,** 1–28.

Brune, J. N. (1970). Tectonic stress and the spectra of seismic shear waves from earthquakes, *J. Geophys. Res.* **75,** 4997–5009.

Cranswick, E., R. W. Wetmiller, and J. Boatwright (1985). High-frequency observations and source parameters of microearthquakes recorded at hard-rock sites, *Bull. Seism. Soc. Am.* **75,** 1535–1567.

Frankel, A. (1982). The effects of attenuation and site response on the spectra of microearthquakes in the northeastern Caribbean, *Bull. Seism. Soc. Am.* **72,** 1349–1402.

Hanks, T. C. (1983). f_{max}, *Bull. Seism. Soc. Am.* **72,** 1867–1879.

Hart, E. W. (1980). Fault-rupture hazard zones in California, *Calif. Div. Mines Geology Spec. Rept. 42,* 25 pp.

Hauksson, E. (1987). Seismotectonics of the Newport-Inglewood fault zone in the Los Angeles Basin, Southern California, *Bull. Seism. Soc. Am.* **77,** 539–561.

Joyner, W. B., R. E. Warrick, and A. A. Oliver, III (1976). Analysis of seismograms from a downhole array in sediments near San Francisco Bay, *Bull. Seism. Soc. Am.* **66,** 937–958.

Kjartansson, E. (1979). Constant Q-wave propagation and attenuation, *J. Geophys. Res.* **84,** 4737–4748.

Klein, F. W. (1985). User's guide to HYPOINVERSE, a program for VAX and PC350 computers to solve for earthquake locations, *U.S. Geol. Surv., Open-File Rept. 85-515*, 24 pp.

Malin, P. E. and J. A. Walker (1985). Preliminary results from vertical seismic profiling of Oroville microearthquake S-waves, *Geophys. Res. Letters* **12,** 137–140.

Newman, P. (1973). Divergence effects in a layered earth, *Geophysics* **38,** 481–488.

Ohtake, M. (1987), Temporal change of Q_p^{-1} in focal area of 1984 western Nagano, Japan, earthquake as derived from pulse width analysis, *J. Geophys. Res.* **92,** 4846–4852.

Papageorgiou, A. S. and K. Aki (1983). A specific barrier model for the quantitative description of inhomogenous faulting and the prediction of strong ground motion. Part I. Description of the model, *Bull. Seism. Soc. Am.* **73,** 693–722.

Phillips, S. W. and K. Aki (1986). Site amplification of coda waves from local earthquakes in central California, *Bull. Seism. Soc. Am.* **76,** 627–648.

Reasenberg, P. and D. Oppenheimer (1986). FPFIT, FPPLOT and FPPAGE: Fortran computer programs for calculating and displaying earthquake fault-plane solutions, *U.S. Geol. Surv., Open-File Rept. 85-739*, 46 pp.

Robinson, E. A. (1983). *Multichannel Time Series Analysis with Digital Computer Programs*, Goose Pond Press, Houston, Texas, 454 pp.

Rogers, A. M., R. D. Borcherdt, P. A. Covington, and D. M. Perkins (1984). A comparative ground response study near Los Angeles using recordings of Nevada nuclear tests and the 1971 San Fernando earthquake, *Bull. Seism. Soc. Am.* **74,** 1925–1949.

Singh, S. K., R. J. Apsel, J. Fried, and J. N. Brune (1982). Spectral attenuation of SH waves along the Imperial fault, *Bull. Seism. Soc. Am.* **72,** 2003–2016.

Stewart, S. W. and M. E. O'Neill (1980). Calculation of the frequency response of the USGS telemetered short-period seismic system, *U.S. Geol. Surv., Open-File Rept. 80-143*, 83 pp.

Takahashi, H., M. Takahashi, H. Suzuki, and M. Ohtake (1984). Deep borehole observation of crustal activity in the metropolitan area of Japan: in *Earthquake Prediction: Proceedings of the International Symposium in Earthquake prediction*, Terra Scientific Publishing Company, Tokyo, Japan, 67–78.

Teng, T.-L. and M. Hsu (1986). A seismic telemetry system of large dynamic range, *Bull. Seism. Soc. Am.* **76,** 1461–1471.

Teng, T.-L., C. R. Real, and T. L. Henyey (1973). Microearthquakes and water flooding in Los Angeles, *Bull. Seism. Soc. Am.* **63,** 859–875.

Tinsley, J. C. and T. E. Fumal (1985). Mapping Quaternary sedimentary deposits for areal variations in shaking response, in *Evaluating Earthquake Hazards in the Los Angeles Region*, J. I. Ziony, Editor, *U.S. Geol. Surv., Profess. Paper 1360*, 101–125.

Yerkes, R. F., T. H. McCulloh, J. E Schoellhamer, and J. G. Vedder (1965). Geology of the Los Angeles basin, California—An introduction, *U.S. Geol. Surv. Profess. Paper 420-A*, A1–A57.

DEPARTMENT OF GEOLOGICAL SCIENCES
UNIVERSITY OF SOUTHERN CALIFORNIA
LOS ANGELES, CALIFORNIA 90089-0740

Manuscript received 12 January 1987